Mechanical mode imaging of a high-Q hybrid hBN/Si_3N_4 resonator

David Jaeger,[†,‡] Francesco Fogliano,[†] Thibaud Ruelle,[†] Aris Lafranca,[‡] Floris Braakman,[†] and Martino Poggio[*,†,‡]

†*Department of Physics, University of Basel, 4056 Basel, Switzerland*

‡*Swiss Nanoscience Institute, University of Basel, 4056 Basel, Switzerland*

E-mail: martino.poggio@unibas.ch

Abstract

We image and characterize the mechanical modes of a 2D drum resonator made of hBN suspended over a high-stress Si_3N_4 membrane. Our measurements demonstrate hybridization between various modes of the hBN resonator and those of the Si_3N_4 membrane. The measured resonance frequencies and spatial profiles of the modes are consistent with finite-element simulations based on an idealized geometry. Spectra of the thermal motion reveal that, depending on the degree of hybridization with modes of the heavier and higher-quality-factor Si_3N_4 membrane, the quality factors and the motional mass of the hBN drum modes can be shifted by orders of magnitude. This effect could be exploited to engineer hybrid drum/membrane modes that combine the low motional mass of 2D materials with the high quality factor of Si_3N_4 membranes for optomechanical or sensing applications.

Keywords

Hexagonal boron nitride; mode imaging; 2D materials; nanomechanical resonators

2D materials enable the fabrication of nanomechanical resonators with high aspect ratios, very low mass, and high resonance frequencies.[1–5] They have remarkable mechanical properties, such as extremely high fracture strength and Young's Modulus.[6] A wide variety of 2D materials are now subject of large research efforts, due to their unique electronic,[7,8] magnetic[9,10] and optical[11,12] features, as well as the potential to combine these materials in layered heterostructures.[13] Hexagonal boron-nitride (hBN) is known to have comparable mechanical properties to graphene,[14] but in contrast to graphene and other 2D materials it has a large bandgap of almost 6 eV,[15] making it a transparent insulator with low absorption in the visible and near infra-red range.[16] hBN has also been shown to host bright and stable quantum emitters,[17] which are strain-coupled to the motion of the crystal lattice.[18,19] These properties make hBN a prime candidate for optomechanical devices and integration into high-finesse optical cavities.[20]

Most devices based on suspended flakes of 2D materials are fabricated by direct exfoliation[1,21] or dry stamping onto a pre-patterned substrate.[22] Due to the thickness of the substrate and the fact that there is usually no optical access from both sides, these samples are not suitable for integration with micro-scale optical cavities in the membrane-in-the-middle (MIM) configuration.[23–25] In addition, mechanical mode imaging on such devices has revealed that these transfer techniques have a deleterious effect on the mode shapes and potentially on the mechanical properties of the resonators, due to the inhomogeneous stress they impart to the flake.[2,26,27] Aside from degrading the overall performance of the devices and their reproducibility, this is also problematic for sensing implementations that require calibrated mode shapes.[26] Suspended devices made from 2D materials grown by chemical vapour deposition are fabricated with wet transfer techniques,[28] but they usually exhibit many folds, cracks or other imperfections that affect the resulting mechanical resonators to a similar degree.[29,30]

In this work, we employ a wet transfer technique to fabricate devices from exfoliated flakes of hBN (Fig. 1 (a)) which are placed on top of holes in Si_3N_4 membranes, resulting

in thin devices with optical access from both sides (Fig. 1 (b)). We characterize such a hBN/Si_3N_4 mechanical resonator by measuring thermal mode spectra, as well as detailed spatial mode shapes. We find that the mode shapes match well with COMSOL Multiphysics simulations based on idealized geometries. Finally, we explore how the hybridization between the mechanical modes of the Si_3N_4 membrane and of the hBN drum affects the mechanical properties of the latter.

While hybridization between 2D material resonators and underlying Si_3N_4 membranes has been observed before,[31,32] here we focus on the changes in the quality factor (Q) and effective mass (m^*). In our case, the underlying Si_3N_4 membrane has a much higher Q than the hBN drum. This results in hybridization where the Si_3N_4 membrane lends its mechanical properties to the modes of the hBN drum, which could be useful for sensing applications,[31,33,34] and the engineering of functionalized mechanical systems.

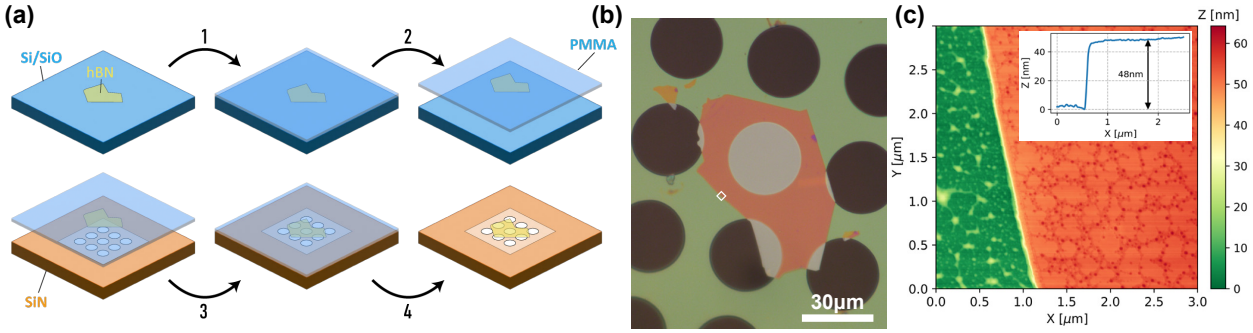

Figure 1: (a) Sample fabrication procedure. hBN flakes are exfoliated onto Si/SiO_2 substrates and then spin-coated with PMMA in step 1. In step 2, the oxide layer is removed, releasing the PMMA layer with embedded hBN flakes. In step 3, this PMMA layer is brought into contact with the Si_3N_4 membrane, producing a hBN drum resonator. Finally, in step 4, the PMMA is removed in a solvent clean. (b) Photograph of a finished sample (c) AFM measurement of the area indicated by the small white rectangle in (b), giving a flake thickness of 48 nm.

Our device fabrication starts with exfoliated hBN flakes (hq-graphene) on a Si/SiO_2 substrate with a 300 nm oxide layer. hBN offers a poor optical contrast on PDMS, which is typically used in stamping techniques.[35] However, on a Si/SiO_2 substrate the flakes can be carefully evaluated and selected, making it possible to find flakes without defects, steps

or folds. The Si/SiO_2 chip is then spin-coated with a layer of Poly(methyl methacrylate) (PMMA), after which the oxide layer is removed in a 2M NaOH solution. This results in a floating PMMA membrane with hBN flakes attached to its bottom surface (see Fig. 1 (a) step 1-2). We have found that a slow etching of the SiO_2 at room temperature yields a smoother and cleaner PMMA membrane compared to a faster process at elevated temperatures, as is often employed. After replacing the NaOH solution with DI water in several rinsing steps, the PMMA/hBN membrane is transferred to another vessel where it floats above the target substrate. This substrate is a stoichiometric (900 MPa stress) Si_3N_4 membrane (Norcada). It is 200 nm thick, has lateral dimensions of 300 µm x 300 µm, and features 30 µm diameter holes in a grid pattern. The Si_3N_4 membrane is glued with Crystalbond to a metal holder so as to not float away or move during the transfer. To position the PMMA membrane on top of the Si_3N_4 chip, we use a micromanipulator setup under an optical microscope. While positioning the hBN flake above the target hole in the Si_3N_4 membrane, the water is slowly removed until the hBN flake settles on top of the hole (Fig. 1 (a) step 3). The device is left to dry over night, after which the PMMA is removed in acetone followed by IPA at 50 °C for 30 min each (Fig. 1 (a) step 4). Finally, the sample is put into a UV/Ozone cleaner for 10 min to remove organic residue.

The characterization of the sample is carried out in a room temperature vacuum chamber (pressure $<10^{-4}$ mbar) with optical access for a modified Michelson interferometer (see Ref. 36). A single-frequency diode laser (630 nm) is used to detect the motion of the hBN drum in a balanced detection scheme. We use a long working distance 50x objective with an NA of 0.5 (Mitutoyo G-Plan Apo 50x) giving us a spot-size of around 800 nm. The length of the reference arm of the interferometer is stabilized via a feedback loop to keep the interferometer stable and at maximum sensitivity throughout the measurements. We also use this length control of the reference arm, which can cover more than the laser wavelength, as calibration to convert from units of $[V^2/Hz]$ to $[m^2/Hz]$. The mechanical response is measured by exciting the sample resonantly with a piezoelectric shaker to an amplitude of a few nm,

while recording the demodulated signal with a lock-in amplifier (Zurich HF2LI). A stack of piezo scanners (Attocube ANSxy50) makes it possible to map the reflected intensity of the sample, as well as to image the mechanical modes as in Fig. 2.

Mode imaging is not only a tool that can give insight into the imperfections (folds, wrinkles, inhomogeneous strain etc.) of the membrane and their effect on the mode shapes, but it also allows to identify to which mode each resonance peak found in the spectrum belongs. This turns out to be particularly useful when the resonance spectrum is not well predicted by theory, or as in our case, is complicated by hybridization of the modes.

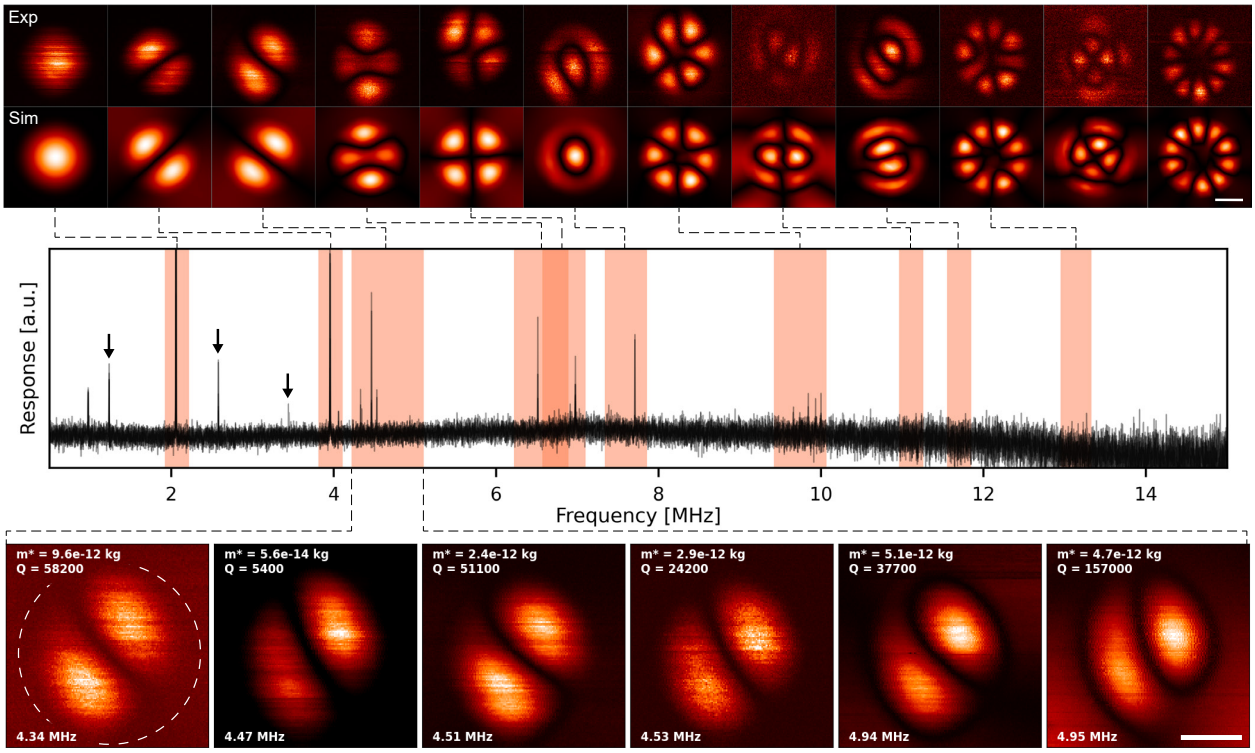

Figure 2: Mode images and spectrum obtained for the sample shown in Fig. 1 (b). Top row shows the measured mode images while the second row shows mode images simulated with COMSOL. Since often more than one mode could be found with matching mode images, the modes are represented with a shaded area rather than with a specific peak in the thermal spectrum shown below. The last two mode images are beyond the frequency range of the thermal spectrum shown, therefore no shaded area is indicated. Arrows highlight modes of the Si_3N_4 membrane that did not hybridize with any hBN drum modes, starting with the fundamental Si_3N_4 mode. The last row shows an example of a series of apparently identical modes in one of the shaded areas. m^*, Q and resonance frequency are displayed on each of the six graphs. Scale bars correspond to 10 µm.

We have characterized and imaged a wide array of mechanical modes visible in the thermal spectrum (Fig. 2) of the sample shown in Fig. 1 (b). This data gives insight into the resonance spectrum and confirms that the mode shapes (first row of images in Fig. 2) match the ones simulated with COMSOL (second row of images in Fig. 2). We can also use the thermal spectra to characterize the mechanical properties of the modes in question, in particular their m^* and Q. For example, the thermal spectrum recorded for the fundamental mode of the hBN drum at around 2 MHz is shown in Fig. 3 (a). The theoretical effective mass $m^*_{th} = 1.89 \times 10^{-14}\,\mathrm{kg}$ agrees with the measured $m^* = 1.71 \times 10^{-14}\,\mathrm{kg}$. For the theoretical value, we assumed a density of hBN of $\rho_{hBN} = 2100\,\mathrm{kg\,m^{-3}}$ and a ratio between m^* and geometrical mass m of $m^*/m = 0.265$.[37] The drum has a diameter of $d = 30\,\mu\mathrm{m}$ and a thickness of $t = 48\,\mathrm{nm}$ (Fig. 1 (c)). To fit the thermal spectra we use the power spectral density

$$S_{xx}(\omega) = \frac{2\Gamma k_B T}{m^*((\omega_0^2 - \omega^2)^2 + \Gamma^2\omega^2)} \tag{1}$$

where $\omega/2\pi$ is the frequency (ω_0 at resonance), $\Gamma = \omega_0/Q$ the linewidth, T the temperature, and k_B the Boltzmann constant. We assume that the sample is thermalized with the surrounding bath. The optical power ($\sim 100\,\mu\mathrm{W}$) was chosen so as to cause a negligible shift in the resonance frequencies of the hBN drum, this was done by increasing the power until a heating effect could be observed and then reducing the power well below that point.

We measure a quality factor $Q = 6250$ for the fundamental mode of the hBN drum. We are not aware of a device with higher Q at room-temperature based on a 2D material. Typically, Q-factors of such devices are in the range of $10^1 - 10^2$.[1,3,21,30,38,39]

We often find several copies of a specific mode shape in a frequency interval indicated by the shaded regions in Fig. 2. An example of a series of such modes with observable thermal motion can be seen in the bottom of Fig. 2. We attribute the presence of such copies to hybridization between an hBN drum mode and several modes of the Si_3N_4 membrane that are close in frequency (see Fig. S3 (c)). We again employ COMSOL simulations to gain more insight into the combined system (Fig. S1). The simulations predict a variety of hybridized

modes where the Ince-Gaussian type modes expected for the hBN drum are combined with modes of the Si_3N_4 membrane.[40] This results in a much larger number of modes compared to a bare hBN drum and also affects the rotational orientation of the hBN drum modes. When taking a closer look at the bottom row in Fig. 2, it becomes apparent that some of the mode images show motion (bright color) surrounding the typical double maxima of the drum mode, hinting at hybridization with the surrounding Si_3N_4 membrane. As expected, the mode with the lowest Q-factor (second image) shows no motion in the surrounding Si_3N_4 membrane, while the one with the highest Q-factor (last image) shows strong motion that even merges with the mode shape of the hBN drum. The fundamental mode of the hBN drum is not expected to show any hybridization (inset Fig. 3 (a)), since it sits in a frequency gap in the mode spectrum just after the fundamental mode of the Si_3N_4 membrane (arrows in Fig. 2, Fig. S3). Instead, for higher order modes of the hBN drum we expect hybridization with modes of the Si_3N_4 membrane based on the simulations.

To further investigate this hybridization, we extract m^* and Q for all the modes observed in the thermal spectrum. We also performed measurements both at liquid nitrogen (77 K) and liquid helium (4 K) temperatures. The sample was cooled in a liquid helium bath cryostat (Cryomagnetics) and measurements were performed using a fiber based microscope as described in Ref. 41.

In Fig. 3 (b) we show Q as a function of the resonance frequency. For a small frequency interval there are often many modes at different Q's that almost appear in a vertical line, representing groups of modes as the one shown at the bottom of Fig. 2. The room-temperature qualtiy factor $Q = 1.8 \times 10^5$ for the Si_3N_4 membrane (see Fig. S3 (a)) is much higher than the one for the fundamental mode of the hBN drum (Fig. 3 (a)). Among the observed thermal spectra whose mode images match modes expected for the hBN drum (e.g Fig. 2 bottom row), we have found Q-factors in excess of 1×10^5, almost reaching the value of the Si_3N_4 membrane.

If the motion that we detect on the hBN drum were coupled to motion in the Si_3N_4, we

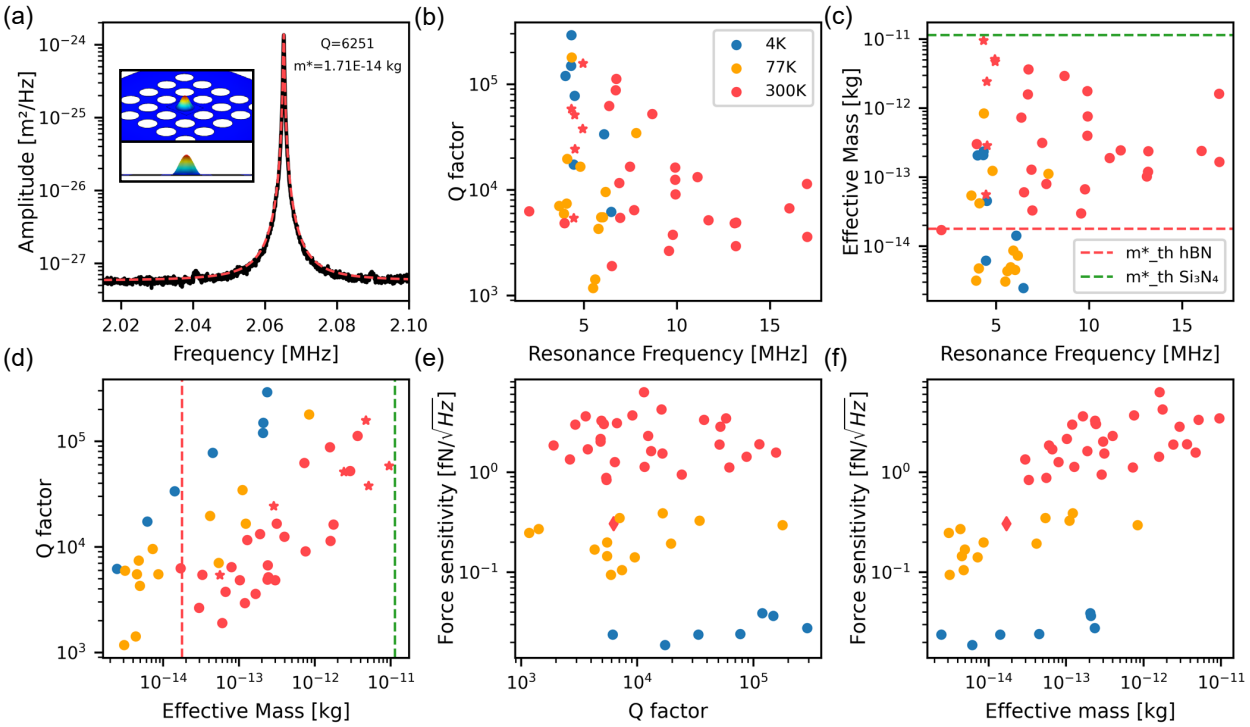

Figure 3: (a) Thermal spectrum of the fundamental mode with fit in red. Q and m^* extracted from this fit are shown to the right of the peak, while the inset to the left shows the expected deflection as simulated with COMSOL. The motion is confined to the hBN that covers the central hole. (b),(c) Q and m^* as a function of the resonance frequency for all observed modes at different temperatures. The six modes shown at the bottom of Fig. 2 are represented with star shaped markers. (d) Q vs. m^*. The dashed lines in (c),(d) indicate m^*_{th} of hBN and Si_3N_4. (e) and (f) show the extracted force sensitivity vs Q and m^*; the diamond shaped markers represent the fundamental hBN mode at room temperature.

would expect an increase in m^* of this hybridized mode, since the Si_3N_4 membrane is a much heavier oscillator. As can be seen in Fig. 3 (c), where we look at m^* instead, we indeed find an increase in these values. The observed values for room temperature (red markers) fall between a lower limit (red dashed line) corresponding to m^*_{th} of the fundamental mode of the hBN drum and an upper limit (green dashed line) corresponding to m^*_{th} of the Si_3N_4 membrane. While these limits are only estimates, especially for the circular hBN drum where the effective mass depends on the mode in question,[37] the behaviour matches our expectations for different degrees of hybridizations. If we plot the observed Q vs. m^* (Fig. 3 (d)), we find that the modes with higher Q tend to have a higher m^*, the two values appear

to be correlated. From this observation we can conclude that, via hybridization, the Si_3N_4 membrane can lend its high Q-factor to the hBN at the cost of a higher effective mass. In Fig. 3 (e) and (f) we show the extracted force sensitivity (see supplementary information). At room temperature, the best value is achieved for the fundamental mode, showing that hybridization does not have a positive effect for this sample. The improvement observed at low temperature is partially due to a drop in effective mass of the observed modes. To explain the shift towards lower m^*, we need to take changes in the resonator geometry during cool-down into account.

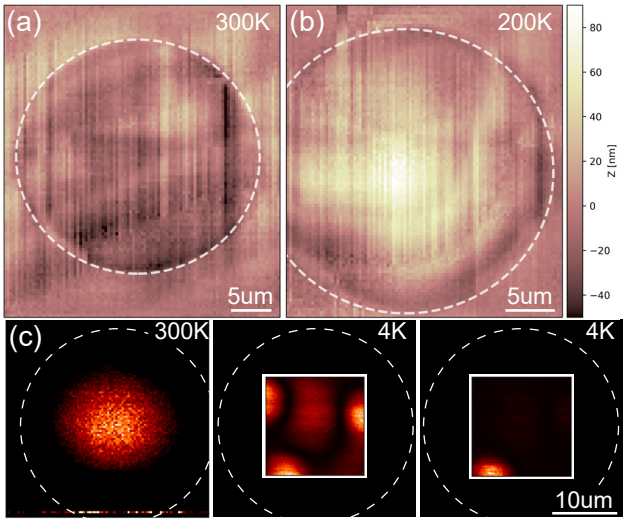

Figure 4: (a),(b) Maps of the height differences extracted from the reflected intensity, showing the bulging effect at lower temperatures. (c) Fundamental hBN mode at room temperature (left), modes of the bulged drum at 4 K (middle, right). The image in the middle shows a complex mode that spans a large area, for which thermal motion could not be observed. The image on the right is a more typical mode representing the ones that we were able to characterize (see Fig. 3). Dashed circles show the drum edge while the white squares in the last two images indicate the limited scan window at 4 K.

Bulk hBN is known to have a negative thermal expansion coefficient,[42] so, as in graphene, it is reasonable to expect that this property is preserved or even enhanced in the 2D limit.[43] Therefore, we expect a bulging of the membranes going to low temperatures. While no such effect was observed for monolayer hBN,[30] the sample presented here is not thin enough to be clearly in the membrane regime, where the drum would be expected to stay under tension by

adhering to the side walls of the underlying substrate.[2] Indeed, we observe buckling for our sample, as can be seen in the reflected intensity maps in Fig. 4 (a) and (b). While we observe an increase in Q (Fig. 3), especially when comparing similar effective masses, the effect is not as big as in other published work.[7,29,30,44] It is difficult to draw clear comparisons since the nature of the mechanical modes significantly changes after the bulging takes place (see Fig. 4 (c)). For example, we can not observe the evolution of the Q-factor of the fundamental mode as a function of temperature, since no corresponding mode exists after buckling.

Looking at Fig. 3, m^* tends towards lower values for lower temperatures, even falling well below the expected value for the fundamental mode of hBN. This is not surprising, as the mode images reveal that a much smaller area of the membrane takes part in the motion for some of the observed modes in the bulged membranes (Fig. 4 (c)). Unlike at room temperature, we do not observe m^* reaching the upper limit given by the motional mass of the Si_3N_4 membrane. We believe that this is due to our inability to observe thermal motion for such modes. The thermal motion scales with T and inversely with m^* and ω (Eq. 1), limiting the range of observable spectra at low temperatures.

To summarize, the device presented here shows excellent mechanical properties and exhibits mode shapes that are consistent with theory up to high mode orders. We believe that the most likely explanation for this good performance is the fabrication procedure. The Si/SiO_2 substrate enables good visibility of any imperfections in the flake and the wet transfer allows the flakes to gently settle onto the Si_3N_4 membrane, avoiding inhomogeneous stress in the drum. While the thickness does not appear to have an effect on the Q of similar devices,[1–3,20,21] there may be a positive effect due to the large drum diameter of our devices.[45] Another factor that is known to influence Q is the tension,[29] which we estimate in our samples to not be any higher compared to similar published work (see supplementary information).[2,7,30]

The hybridization between the Si_3N_4 membrane and the hBN drum not only boosts the Q of the hBN modes, it also allows the selection of different values of Q (m^*), because the

hybridization splits the expected hBN modes into several copies with different degrees of hybridization. With the addition of temperature control it should be possible to tune this hybridization in a similar way as in Ref. 31,32.

While the gain in Q does not outweigh the increase in m^* when estimating the sensitivity of our devices (Fig. 3 and S2), Si_3N_4 membranes with higher Q or lower m^* have been demonstrated and could make this trade-off more favorable.[46,47] In particular, since the placement of hBN on our membranes resulted in only a modest drop in Q of the fundamental mode (see supplementary information), we are optimistic that hybrid modes with much higher Qs are feasible. Schwarz et al. demonstrated theoretically and experimentally that hybridization can increase thermally-limited sensitivity in a similar system.[31] Crucially, this increase in sensitivity requires the fine tuning of the two modes to be hybridized, implying the need of a specifically designed Si_3N_4 membrane for the task. Hybridization of a Si_3N_4 resonator with a 2D membrane can also boost its motional amplitude allowing for larger optomechanical coupling in a cavity or giving access to non-linear mechanical effects such as signal amplification and noise squeezing.[4,32,34] The ability to study high-Q mechanical modes in 2D materials also opens possibilities for studying their mechanical properties, for mechanical coupling to embedded quantum emitters, or even for measuring magnetic properties of 2D materials via the magnetic torques and forces acting on drum resonators made from 2D magnets or on 2D magnets encapsulated in suspended hBN drum resonators.

Acknowledgement

We thank Sascha Martin and his team in the machine shop of the Physics Department at the University of Basel for help in building the apparatus. We acknowledge the support of the Canton Aargau and the Swiss National Science Foundation (SNSF) under Ambizione Grant No. PZ00P2-161284/1 and Project Grant No. 200020-178863 and via the NCCR Quantum Science and Technology (QSIT).

Supporting Information Available

- SuppInfo.pdf: COMSOL simulations; Force and mass sensitivity estimates; Mechanical properties of the Si_3N_4 membrane.

References

(1) Bunch, J. S.; van der Zande, A. M.; Verbridge, S. S.; Frank, I. W.; Tanenbaum, D. M.; Parpia, J. M.; Craighead, H. G.; McEuen, P. L. Electromechanical Resonators from Graphene Sheets. *Science* **2007**, *315*, 490–493

.

(2) Zheng, X.-Q.; Lee, J.; Feng, P. X.-L. Hexagonal Boron Nitride Nanomechanical Resonators with Spatially Visualized Motion. *Microsystems & Nanoengineering* **2017**, *3*, 17038

.

(3) Castellanos-Gomez Andres,; van Leeuwen Ronald,; Buscema Michele,; van der Zant Herre S. J.,; Steele Gary A.,; Venstra Warner J., Single-Layer MoS2 Mechanical Resonators. *Advanced Materials* **2013**, *25*, 6719–6723

.

(4) Steeneken, P. G.; Dolleman, R. J.; Davidovikj, D.; Alijani, F.; van der Zant, H. S. J. Dynamics of 2D Material Membranes. *2D Materials* **2021**, *8*, 042001

.

(5) Xu, B. et al. Nanomechanical Resonators: Toward Atomic Scale. *ACS Nano* **2022**, *16*, 15545–15585

.

(6) Lee, C.; Wei, X.; Kysar, J. W.; Hone, J. Measurement of the Elastic Properties and Intrinsic Strength of Monolayer Graphene. *Science* **2008**, *321*, 385–388

.

(7) Chen, C.; Rosenblatt, S.; Bolotin, K. I.; Kalb, W.; Kim, P.; Kymissis, I.; Stormer, H. L.; Heinz, T. F.; Hone, J. Performance of Monolayer Graphene Nanomechanical Resonators with Electrical Readout. *Nature Nanotechnology* **2009**, *4*, 861–867

.

(8) Chen, C.; Lee, S.; Deshpande, V. V.; Lee, G.-H.; Lekas, M.; Shepard, K.; Hone, J. Graphene Mechanical Oscillators with Tunable Frequency. *Nature Nanotechnology* **2013**, *8*, 923–927

.

(9) Gong, C.; Li, L.; Li, Z.; Ji, H.; Stern, A.; Xia, Y.; Cao, T.; Bao, W.; Wang, C.; Wang, Y.; Qiu, Z. Q.; Cava, R. J.; Louie, S. G.; Xia, J.; Zhang, X. Discovery of Intrinsic Ferromagnetism in Two-Dimensional van Der Waals Crystals. *Nature* **2017**, *546*, 265–269

.

(10) Huang, B.; Clark, G.; Navarro-Moratalla, E.; Klein, D. R.; Cheng, R.; Seyler, K. L.; Zhong, D.; Schmidgall, E.; McGuire, M. A.; Cobden, D. H.; Yao, W.; Xiao, D.; Jarillo-Herrero, P.; Xu, X. Layer-Dependent Ferromagnetism in a van Der Waals Crystal down to the Monolayer Limit. *Nature* **2017**, *546*, 270–273

.

(11) Splendiani, A.; Sun, L.; Zhang, Y.; Li, T.; Kim, J.; Chim, C.-Y.; Galli, G.; Wang, F. Emerging Photoluminescence in Monolayer MoS2. *Nano Letters* **2010**, *10*, 1271–1275

.

(12) Srivastava, A.; Sidler, M.; Allain, A. V.; Lembke, D. S.; Kis, A.; Imamoğlu, A. Optically Active Quantum Dots in Monolayer WSe2. *Nature Nanotechnology* **2015**, *10*, 491–496

.

(13) Novoselov, K. S.; Mishchenko, A.; Carvalho, A.; Castro Neto, A. H. 2D Materials and van Der Waals Heterostructures. *Science* **2016**, *353*, aac9439

.

(14) Falin, A.; Cai, Q.; Santos, E. J. G.; Scullion, D.; Qian, D.; Zhang, R.; Yang, Z.; Huang, S.; Watanabe, K.; Taniguchi, T.; Barnett, M. R.; Chen, Y.; Ruoff, R. S.; Li, L. H. Mechanical Properties of Atomically Thin Boron Nitride and the Role of Interlayer Interactions. *Nature Communications* **2017**, *8*, 15815

.

(15) Watanabe, K.; Taniguchi, T.; Kanda, H. Direct-Bandgap Properties and Evidence for Ultraviolet Lasing of Hexagonal Boron Nitride Single Crystal. *Nature Materials* **2004**, *3*, 404–409

.

(16) Lee, S.-Y.; Jeong, T.-Y.; Jung, S.; Yee, K.-J. Refractive Index Dispersion of Hexagonal Boron Nitride in the Visible and Near-Infrared. *physica status solidi (b)* **2019**, *256*, 1800417

.

(17) Tran, T. T.; Bray, K.; Ford, M. J.; Toth, M.; Aharonovich, I. Quantum Emission from Hexagonal Boron Nitride Monolayers. *Nature Nanotechnology* **2016**, *11*, 37–41

.

(18) Mendelson, N.; Doherty, M.; Toth, M.; Aharonovich, I.; Tran, T. T. Strain-Induced Modification of the Optical Characteristics of Quantum Emitters in Hexagonal Boron Nitride. *Advanced Materials* **2020**, *32*, 1908316

.

(19) Lazić, S.; Espinha, A.; Yanguas, S. P.; Gibaja, C.; Zamora, F.; Ares, P.; Chhowalla, M.; Paz, W. S.; Burgos, J. J. P.; Hernández-Mínguez, A.; Santos, P. V.; van der Meulen, H. P. Dynamically Tuned Non-Classical Light Emission from Atomic Defects in Hexagonal Boron Nitride. *Communications Physics* **2019**, *2*, 1–8

.

(20) Shandilya, P. K.; Fröch, J. E.; Mitchell, M.; Lake, D. P.; Kim, S.; Toth, M.; Behera, B.; Healey, C.; Aharonovich, I.; Barclay, P. E. Hexagonal Boron Nitride Cavity Optomechanics. *Nano Letters* **2019**, *19*, 1343–1350

.

(21) Lee, J.; Wang, Z.; He, K.; Shan, J.; Feng, P. X.-L. High Frequency MoS2 Nanomechanical Resonators. *ACS Nano* **2013**, *7*, 6086–6091

.

(22) Castellanos-Gomez, A.; Buscema, M.; Molenaar, R.; Singh, V.; Janssen, L.; van der Zant, H. S. J.; Steele, G. A. Deterministic Transfer of Two-Dimensional Materials by All-Dry Viscoelastic Stamping. *2D Materials* **2014**, *1*, 011002

.

(23) Ruelle, T.; Jaeger, D.; Fogliano, F.; Braakman, F.; Poggio, M. A Tunable Fiber Fabry–Perot Cavity for Hybrid Optomechanics Stabilized at 4 K. *Review of Scientific Instruments* **2022**, *93*, 095003

.

(24) Flowers-Jacobs, N. E.; Hoch, S. W.; Sankey, J. C.; Kashkanova, A.; Jayich, A. M.; Deutsch, C.; Reichel, J.; Harris, J. G. E. Fiber-Cavity-Based Optomechanical Device. *Applied Physics Letters* **2012**, *101*, 221109

.

(25) Rochau, F.; Sánchez Arribas, I.; Brieussel, A.; Stapfner, S.; Hunger, D.; Weig, E. M. Dynamical Backaction in an Ultrahigh-Finesse Fiber-Based Microcavity. *Physical Review Applied* **2021**, *16*, 014013

.

(26) Davidovikj, D.; Slim, J. J.; Bueno, S. J. C.; van der Zant, H. S. J.; Steeneken, P. G.; Venstra, W. J. Visualizing the Motion of Graphene Nanodrums. *Nano Letters* **2016**, *16*, 2768–2773

.

(27) Garcia-Sanchez, D.; van der Zande, A. M.; Paulo, A. S.; Lassagne, B.; McEuen, P. L.; Bachtold, A. Imaging Mechanical Vibrations in Suspended Graphene Sheets. *Nano Letters* **2008**, *8*, 1399–1403

.

(28) Reina, A.; Jia, X.; Ho, J.; Nezich, D.; Son, H.; Bulovic, V.; Dresselhaus, M. S.; Kong, J. Large Area, Few-Layer Graphene Films on Arbitrary Substrates by Chemical Vapor Deposition. *Nano Letters* **2009**, *9*, 30–35

.

(29) van der Zande, A. M.; Barton, R. A.; Alden, J. S.; Ruiz-Vargas, C. S.; Whitney, W. S.; Pham, P. H. Q.; Park, J.; Parpia, J. M.; Craighead, H. G.; McEuen, P. L. Large-Scale Arrays of Single-Layer Graphene Resonators. *Nano Letters* **2010**, *10*, 4869–4873

.

(30) Cartamil-Bueno, S. J.; Cavalieri, M.; Wang, R.; Houri, S.; Hofmann, S.; van der Zant, H. S. J. Mechanical Characterization and Cleaning of CVD Single-Layer h-BN Resonators. *npj 2D Materials and Applications* **2017**, *1*, 16

.

(31) Schwarz, C.; Pigeau, B.; Mercier de Lépinay, L.; Kuhn, A. G.; Kalita, D.; Bendiab, N.;

Marty, L.; Bouchiat, V.; Arcizet, O. Deviation from the Normal Mode Expansion in a Coupled Graphene-Nanomechanical System. *Physical Review Applied* **2016**, *6*, 064021

.

(32) Singh, R.; Sarkar, A.; Guria, C.; Nicholl, R. J.; Chakraborty, S.; Bolotin, K. I.; Ghosh, S. Giant Tunable Mechanical Nonlinearity in Graphene–Silicon Nitride Hybrid Resonator. *Nano Letters* **2020**, *20*, 4659–4666

.

(33) Reiche, C. F.; Körner, J.; Büchner, B.; Mühl, T. Introduction of a Co-Resonant Detection Concept for Mechanical Oscillation-Based Sensors. *Nanotechnology* **2015**, *26*, 335501

.

(34) Singh, R.; Nicholl, R. J.; Bolotin, K. I.; Ghosh, S. Motion Transduction with Thermomechanically Squeezed Graphene Resonator Modes. *Nano Letters* **2018**, *18*, 6719–6724

.

(35) Zheng, X.-Q.; Lee, J.; Feng, P. X.-L. Hexagonal Boron Nitride (h-BN) Nanomechanical Resonators with Temperature-Dependent Multimode Operations. 2015 Transducers - 2015 18th International Conference on Solid-State Sensors, Actuators and Microsystems (TRANSDUCERS). 2015; pp 1393–1396

.

(36) Barg, A.; Tsaturyan, Y.; Belhage, E.; Nielsen, W. H. P.; Møller, C. B.; Schliesser, A. Measuring and Imaging Nanomechanical Motion with Laser Light. *Applied Physics B* **2017**, *123*, 8

.

(37) Hauer, B. D.; Doolin, C.; Beach, K. S. D.; Davis, J. P. A General Procedure for Ther-

momechanical Calibration of Nano/Micro-Mechanical Resonators. *Annals of Physics* **2013**, *339*, 181–207

.

(38) van Leeuwen, R.; Castellanos-Gomez, A.; Steele, G. A.; van der Zant, H. S. J.; Venstra, W. J. Time-Domain Response of Atomically Thin MoS2 Nanomechanical Resonators. *Applied Physics Letters* **2014**, *105*, 041911

.

(39) Kramer, E.; van Dorp, J.; van Leeuwen, R.; Venstra, W. J. Strain-Dependent Damping in Nanomechanical Resonators from Thin MoS2 Crystals. *Applied Physics Letters* **2015**, *107*, 091903

.

(40) Bandres, M. A.; Gutiérrez-Vega, J. C. Ince–Gaussian Modes of the Paraxial Wave Equation and Stable Resonators. *Journal of the Optical Society of America A* **2004**, *21*, 873

.

(41) Högele, A.; Seidl, S.; Kroner, M.; Karrai, K.; Schulhauser, C.; Sqalli, O.; Scrimgeour, J.; Warburton, R. J. Fiber-Based Confocal Microscope for Cryogenic Spectroscopy. *Review of Scientific Instruments* **2008**, *79*, 023709

.

(42) Paszkowicz, W.; Pelka, J.; Knapp, M.; Szyszko, T.; Podsiadlo, S. Lattice Parameters and Anisotropic Thermal Expansion of Hexagonal Boron Nitride in the 10–297.5 K Temperature Range. *Applied Physics A* **2002**, *75*, 431–435

.

(43) Yoon, D.; Son, Y.-W.; Cheong, H. Negative Thermal Expansion Coefficient of Graphene Measured by Raman Spectroscopy. *Nano Letters* **2011**, *11*, 3227–3231

.

(44) Morell, N.; Reserbat-Plantey, A.; Tsioutsios, I.; Schädler, K. G.; Dubin, F.; Koppens, F. H. L.; Bachtold, A. High Quality Factor Mechanical Resonators Based on WSe2 Monolayers. *Nano Letters* **2016**, *16*, 5102–5108

.

(45) Barton, R. A.; Ilic, B.; van der Zande, A. M.; Whitney, W. S.; McEuen, P. L.; Parpia, J. M.; Craighead, H. G. High, Size-Dependent Quality Factor in an Array of Graphene Mechanical Resonators. *Nano Letters* **2011**, *11*, 1232–1236

.

(46) Tsaturyan, Y.; Barg, A.; Polzik, E. S.; Schliesser, A. Ultracoherent Nanomechanical Resonators via Soft Clamping and Dissipation Dilution. *Nature Nanotechnology* **2017**, *12*, 776–783

.

(47) Reetz, C.; Fischer, R.; Assump ç ao, G.; McNally, D.; Burns, P.; Sankey, J.; Regal, C. Analysis of Membrane Phononic Crystals with Wide Band Gaps and Low-Mass Defects. *Phys. Rev. Appl.* **2019**, *12*, 044027

.

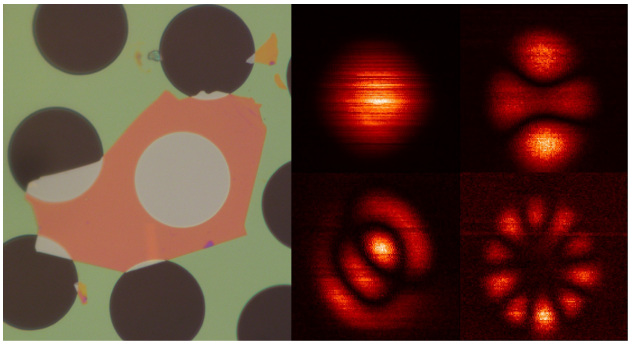

TOC Graphic